Combination of 3D MRI and connectivity analysis in structural evaluation of cancellous bone in rat proximal femur

J. TIMONEN[1], K. KIPPO[2], R. GLANTZ[3], T. PAKKANEN[1]
[1]*University of Joensuu, Department of Chemistry, P.O. Box 111, FIN-80140 Joensuu, Finland*
[2]*Leiras Oy, Biomedical Research Center, P.O. Box 415, FIN-20101 Turku, Finland*
[3]*Vienna University of Technology, Institute of Automation – Pattern Recognition and Image Processing Group, Treitlstr. 3, A-1040 Wien, Austria*

Three dimensional (3-D) magnetic resonance (MR) microimaging combined with connectivity analysis was tested in the study of the structure of cancellous bone. MR microimaging was performed *in vitro* with an average resolution of 20*20*35 μm. A 3-D connectivity analysis was used to model the trabecular bone as a network consisting of nodes and struts. Size distribution curves of these two structural elements and the interconnectivity of nodes was used to estimate the cancellous structure.

The analysis suggested the occurrence of two simultaneous network structures in cancellous bone differed by the size of details. The degradative effect of ostcopenia is found to be slightly different in these two subsystems. Interconnectivity is seen to increase with the size of a node and the expected loss of connectivity due to ostcopenia is observed.

The method described offers a new way in the topological estimation of interconnected medium.

1. Introduction

The expected lifetime will be continuously prolonged in future. This will lead to an extensive increase in the number of patients suffering age-related diseases. Osteoporosis is a typical disease of old age, especially with female patients, and the prognosis predicts the occurrence of osteoporotic bone fractures in one third of women over 65 years [1, 2]. Age-related geometrical change is found in the cross-section of the femoral neck, which shows cancellous bone loss and cortical thinning [3, 4]. The appearance of osteoporosis in elderly women is usually connected to a decrease in physical activity and to estrogen depletion after menopause. As the bone, usually hip, fractures cause remarkable costs both physiologically and financially, the need for new preventing medications is clear. Animal testing is still needed during drug development and the currently accepted model for estrogen-deficiency induced osteopenia is an ovariectomized (OVX) rat model [5]. Currently the standard method for analysis of bone mass and architecture is histomorphometry which uses image analysis from undecalcified and sliced samples [6]. The problem with bone histomorphometry is that collecting sufficient amounts of slice data to reconstruct a true three-dimensional (3-D) presentation is both time consuming and laborious. For this reason, direct 3-D imaging methods may offer an alternative route for analysis of cancellous bone. In this, X-ray tomographic microscope has been successfully applied [7]. This paper presents a combined microscopic range magnetic resonance imaging (MRI) and connectivity analysis study on the effect of ovariectomy and 6 months clodronate treatment on the proximal femur in rats. The histomorphometric data on the effect of clodronate on femoral mid-neck cross-sections in established bone loss of OVX rats has been previously presented elsewhere [8].

2. Material and methods

Female Sprague-Dawley rats were bilaterally ovariectomized (OVX) according to Waynforth [9] or sham-operated (SHAM) at six months of age and were left untreated for the first four months after surgery to allow establishment of cancellous osteopenia [8]. Clodronate treatment (CL, Bonefos®, Leiras Oy, Finland) was initiated in OVX rats at ten months of age. The first treatment group was injected subcutaneously (s.c.) with low dose (1.5 mg/kg/week) of clodronate (C1A) for six months and the second treatment group with high-dose (12.5 mg/kg/week) of clodronate (C1B) for six months. Clodronate dosage was adjusted to body weight changes once a week, the cumulative doses of both regimens being 36 and 300 mg/kg, respectively. The rats were fed with standard small-animal laboratory food (R/M1, SDS Ltd, Witham, UK) containing 0.71% calcium, 0.50% phosphorus and 0.60 IU/g of vitamin D_3, and they had free access to tap water. The rats were housed in individual cages at constant temperature (21 ± 1 °C) and

humidity (45%–55%), using a 12 h light and darkness cycle. Their body weight was measured at the time of operation and weekly thereafter. The local ethical committee in Turku approved the study protocol.

Three randomly selected rats from both basal SHAM and OVX groups sacrificed four months after surgery and two randomly selected rats from both clodronate treatment groups sacrificed at the age of 16 months were used. The proximal end of the right femur was taken and stored undecalcified in 70% ethanol until used for further MR microscopy studies. Prior to MR experiments the ethanol was washed out with water and the bone sample was immersed in water in an MR tube. The possible trapped air was removed from sample by vacuum.

2.1. MR setup

^{1}H MR microscopy experiments were performed on a Bruker AMX-400 NMR spectrometer equipped with an imaging probehead with vertical 5 mm rf coil. A typical value of magnetic field gradient in setup was 30 G/cm. Three dimensional imaging was carried out using 3-D spin echo pulse sequence with: TE (time-to-echo) of 4.37 ms, TR (relaxation delay) of 500 ms, FoV (field of view) of (x-,y-direction) 5 mm (z-direction) 8–10 mm, a data matrix size 256^3 and an experimental time of 55 h. In a typical case a sweep width of 80 kHz was used and the half width of ^{1}H signal in frequency spectrum was 120 Hz.

Connectivity analysis using the ConAn program was made for selected subvolumes containing cancellous bone of primary and secondary spongiosa. Hypointense part of images, i.e. solid bone was modeled as a connectivity network constructed from connectivity centers and connecting throats, nodes and struts, respectively. Spherical structure elements, spheres and cylinders, were used.

Two dimensional relaxation experiments used single slice spin echo sequences with hard exciting and soft refocusing pulse. In T_1 relaxation constant mapping with saturation recovery the experimental parameters were: TE 4.79 ms, TR 150, 300, 600, 1000, 3000 ms, FoV (x, y) 5 mm, in-plane resolution 78 μm, slice resolution 200 μm, data matrix 128^2, with a total experimental time of 45 min. In T_2 relaxation constant mapping parameters were: TE 4.79, 7, 12, 20, 40 ms, TR 2000 ms, FoV and data matrix as in the case of T_1, with a total experimental time of 90 min.

3. Results

3.1. 3-D imaging

The resolution of an image is a crucial factor when the three dimensional structure of porous media is visualized. In MR microimaging the size of the data matrix is usually limited to 256 pixels in each dimension. After this the experimental time increases hugely and the size of digitized data makes processing ineffective. In cancellous bone of rat proximal femur the size of trabeculae is expected to be in the scale of tens of micrometers [8, 10, 11]. As the 3-D spin echo pulse sequence measures over the total volume of a sample, the field of view, or the size of the sample, is limited below 1 cm^3.

In our 3-D experiments the FoV was typically 5*5*9 mm^3, which yields image resolution of 19.5*19.5*35.2 μm^3. Relaxation delay of 500 ms produces slightly T_1 weighted images, where the loss of signal is noteworthy only in bulk water volumes outside the bone. Six scans were coadded to collect enough signal-to-noise for the aforementioned microscopy range voxels (volume cells).

Fig. 1 (a)–(d) presents slices from the center of 3-D images of samples SHAM 1, OVX 4, C1A 7 and C1B 10. The solid bone contains only minor amounts of protons or the mobility of protons is greatly reduced. Using a spin-echo experiment the mobile phase has the major contribution to the echo signal [12]. The volumes of solid material produce no significant MR intensity and are visualized hyperintense after color scale inversion in Fig. 1. The water in cancellous bone region and in volumes surrounding bone gives signal and is seen hypointense. The ostensible higher ^{1}H intensity of cancellous bone region compared to the surrounding region is a T_1 weighing effect and rises from surface induced relaxation inside porous media.

The small number of samples does not justify a sound statistical analysis of the effect of ovariectomy or drug treatment on the structure of bone. On the other hand, a clear connection between ovariectomy and degradation of cancellous bone structure is seen already at four months after OVX. The sample of OVX 4 (Fig. 1(b)) has seemingly lost interconnectivity and cancellous bone mass compared to SHAM 1 (Fig. 1(a)). The degradation is especially clear in the regions of femoral head and neck where the cancellous bone is clearly lost in the OVX class compared to the reference sample of the SHAM group.

Fig. 1(c) and (d) (C1A 7, C1B 10) show the preservative effect of a six month clodronate treatment on the proximal femur. In the regions of the femoral epiphysis bone is dense and closely resembles the OVX sample demonstrating the maintaining effect of the medication. The same observation is done at the cortical bone in the neck region. The different clodronate dosage in the groups C1A and C1B (1.5 mg/kg/week and 12.5 mg/kg/week, respectively) is not observed to produce significant changes in the structure of the proximal femur.

The actual benefit of 3-D imaging is that the slice image data can be manipulated to a volume presentation. In surface reconstruction an intensity level selects volume elements to an image. Data voxels that have shared edges are combined to form a 3-D surface cluster. In our study the threshold intensity for surface rendering was selected to accept only the solid phase and all data voxels of open pores and surrounding water were cut out. An exemplary surface reconstruction of femoral head showing solid material is presented in Fig. 2(a). Surface rendering, being 3-D data, can be further cut to highlight the interesting volumes. Fig. 2(b) shows a small fraction of trabecular architecture from the femoral neck of ovariectomized sample (OVX 4) with a subcube size of 16*48*16 data voxels (0.155 mm^3). For further processing we selected hexahedral subvolumes from a region inside proximal femur between the growth plate and the

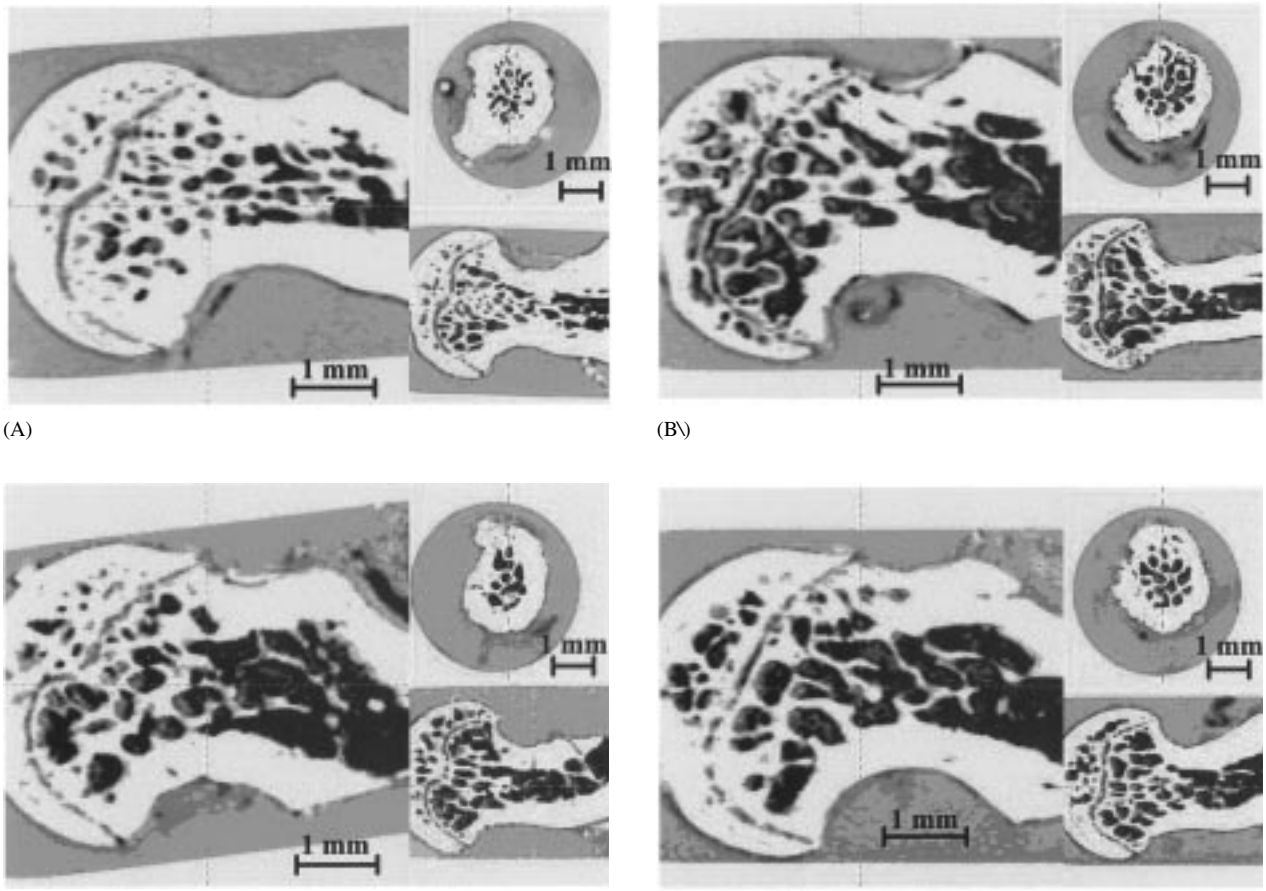

(A) (B\) (C) (D)

Figure 1 Longitudinal and cross-sectional images illustrating the proximal femur in SHAM (A) and OVX (B) rats at four months after surgery, and in OVX rats treated s.c. once a week for six months with clodronate at dose levels of 1.5 mg/kg (C) or 12.5 mg/kg (D). The dotted lines indicate the site of the proximal femur where the longitudinal and cross-sections were taken. The trabecular network in the SHAM group is denser and better connected than in the OVX group.

neck. The sizes of subvolumes varied between 0.49–2.63 mm^3 and contained only cancellous bone.

Surface representation gives the volume of the selected phase in voxel units. Relative cancellous bone volume (BV/TV) was calculated by dividing the volume of surface rendering with the total volume of original hexahedral subvolume. The calculated percentage values can be found in Table I. As expected from the visual observations of the sample classes C1A and C1B, no significant differences between the classes were found and they have been joined for the mean value.

According to Table I the deviation in cancellous bone volume is large in each group. As the needs for instrumental time prevent extensive experimental series the statistical significance of the results remains quite modest. Some trendlines can still be seen. In SHAM-operated samples the mean relative cancellous bone volume is 50% and it is clearly bigger than in OVX or CL samples (34% and 33%, respectively). Clodronate treatment in CL samples preserves bone both in the cortical region and cancellous bone in the epiphysis of the proximal femur as already shown in Fig. 1(c) and (d).

When the surface rendering is applied on the whole data set a healthy bone should be constructed of one single cluster. During osteopenia the interconnecting trabeculae may be totally dissolved creating isolated structures. In this case a fragment is floating free in bone marrow with no true supporting effect. In our samples the surface rendering found loose fragments in all ovariectomized samples and one minor splinter in the SHAM 3 sample (Table I). According to surface rendering the mean amount of isolated cancellous bone structures in osteopenic bone was 0.22%.

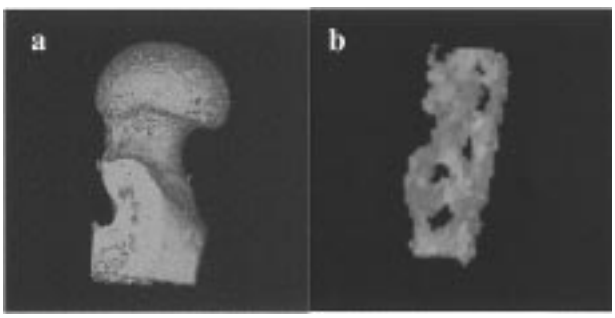

Figure 2 Surface reconstructions of femoreal head (a) and a separated small subcube containing cancellous bone (b) of sample OVX 6.

3.2. 3-D connectivity analysis

The selected subcubes of surface reconstruction were further used for connectivity analysis using program ConAn [13, 14]. Basically it transforms the foreground of a binary 3-D image into a network consisting of connectivity centers and connecting throats. The threshold intensity was selected to push the hyperintense volume i.e. the immersed water (the former marrow) into background and to use hypointense volume, the solid trabeculae as foreground. Spherical structure elements

TABLE I Results from surface rendered 3-D images

	FoV* (mm^3)	VOI† (mm^3)	BV/TV% (%)	Mean BV/TV% (%)	Loose fragments of BV/TV%
Sham 1	9*5*5	0.985	40.9		—
Sham 2	9*5*5	0.657	45.4		—
Sham 3	8*5*5	1.168	62.9	50	0.02%
Ovx 4	9*5*5	2.628	24.2		0.34%
Ovx 5	8*5*5	2.226	41.5		0.14%
Ovx 6	8,5*5*5	0.931	36.2	34	0.19%
C1A 7	10*5*5	0.487	32.8		—
C1A 8	8*5*5	1.314	33.7		—
C1B 9	9*5*5	0.985	30.4		—
C1B 10	8*5*5	0.876	35.1	33	—

*FoV = Field of view; the size of the measured volume.
†VOI = Volume of interest; the size of hexagon used for BV/TV% estimation.

were used, meaning that the connectivity centers, or nodes, were modeled as spheres and the connecting throats, or struts, as cylinders. A schematic presentation of network model is shown in Fig. 3.

From the output data three representitve distributions were chosen. The number of nodes with respect to the size of node and the number of struts with respect to the width of strut are presented in Fig. 4(a) and (b), respectively. The mean coordination number with respect to the size of the node is presented in Fig. 5.

The original output of connectivity analysis gives distribution values, which are correlated to image voxels. As the size of a voxel varies between experiments, the size (width) of structural element was converted from number of voxels to μm. Each original distribution was fitted to a gaussian model. Models were scaled to the same distribution curve area. These models of each sample class were combined to give a mean fit distribution to describe the status of trabecular architecture.

The size distributions of structural elements are presented in Fig. 4. In a homogeneous porous media a single gaussian size distribution of structural elements is expected. However, in all cases of connectivity centers and throats two seperate gaussian functions *A* and *B* were needed to fit size distributions satisfactorily. In case of nodes the distribution *A* maxima have values of node

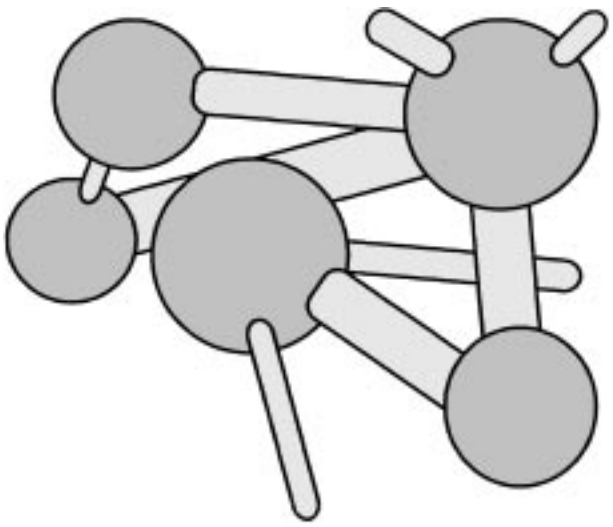

Figure 3 A schematic presentation of model network consisting of spherical connectivity centers (nodes) and cylindrical connecting throats (struts).

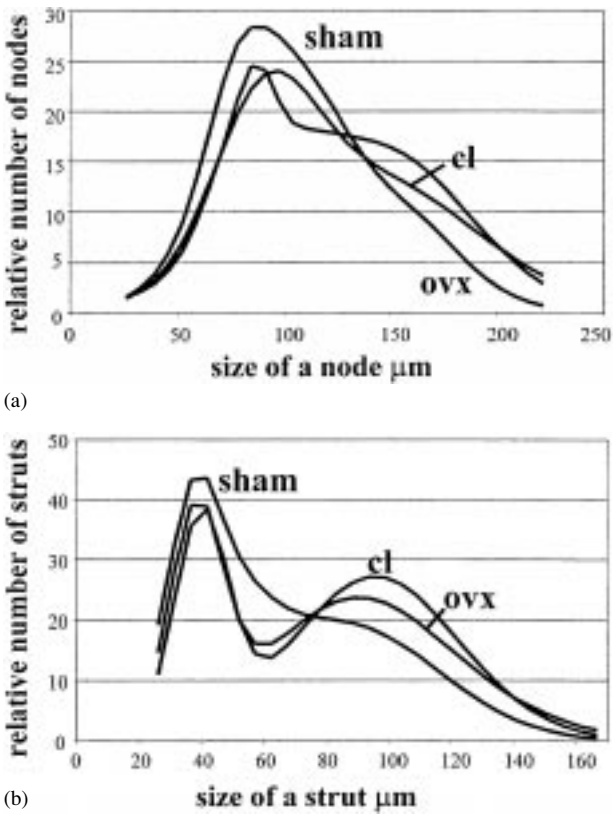

Figure 4 Size distribution curves for connectivity nodes (a) and connecting struts (b) in cancellous bone from connectivity analysis.

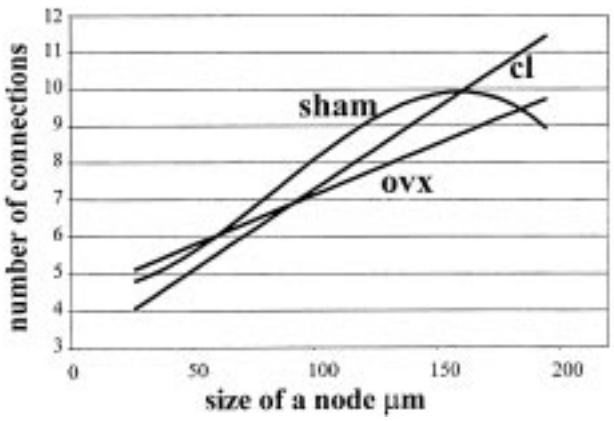

Figure 5 Mean number of trabecular connections with respect to the size of a node in each sample class.

sizes 85, 90, and 84 μm and distribution *B* maxima of sizes 125, 146, and 136 μm for SHAM, OVX and CL, respectively. In the case of connecting struts the maxima *A* are located at strut widths 39, 38, and 40 μm and the maxima *B* at widths 75, 91, and 96 μm for SHAM, OVX, and CL, respectively. The mean size distribution data is presented in Tables II and III.

This suggests that two simultaneous structurally different trabecular occur at volume of interest. The selected volumes of interest contained both primary and secondary spongiosa of trabecular structure and we are quite tempted to say that the trabecular system *A* of smaller size distributions is primary spongiosa and the system *B* of larger structural sizes is the metabolically more mature secondary part of trabecular bone. In principle the anisotropy of trabecular bone reported, e.g. by Kothari *et al*. [15] should produce similar observations of different size distributions for connecting throats. In the case of trabecular anisotropy the size distribution of connectivity centers should, however, be explainable by a single gaussian model. This supports the occurrence of two structurally differing trabecular systems.

The surface constructs stated that the mean trabecular volume was 50% in SHAM group, 34% in OVX, and 33 in CL. In Fig. 4 (a) and (b) the general shape of the size distributions of structural elements is relatively similar in all sample classes and osteopenia is found to degrade both systems *A* and *B*. Sample classes OVX and CL resemble each other quite closely. The mean structural size of system *A* is not affected by osteopenia indicating that the total subsystem *A* suffers uniformly from bone loss. The mean structural sizes of subsystem *B* differ between classes SHAM and OVX-CL. In ovariectomized and treated samples the fragment size is increased compared to the healthy reference. This means that osteopenia tends to decompose subsystem *B* mainly from the smaller fragments leading to relative increase in the trabecular width.

Fig. 5 presents ConAn results where the mean number of trabecular connections, or the coordination number, is plotted with respect to the size of connectivity center. Quite logically the mean number of connections increases with the size of the center. Due to the small number of samples the standard deviations of the mean fits are relatively large (1.6–1.9 connections in all sample classes) and statistically all of the line fits lay inside the error limits of the other line fits. A qualitative survey on the effect of osteopenia may, however, be done and the interconnectivity is seen to decrease by an average of 1.5 connections regardless of the size of a center.

3.3. Relaxation time mapping

The transverse relaxation time T_2 of adsorbed liquid in porous media is known to reflect the pore size distribution of the solid [16, 17] and the smaller the pore, the faster should the relaxation of adsorbate be. As the osteoporotic degradation of bone progresses, the pore size distribution in cancellous bone should change to larger openings. The observativity of this effect in T_1 and T_2 relaxation time mapping was tested with all samples.

The trabecular matrix is however structurally too heterogeneous to find a correlation between mean relaxational characteristics and mean pore size. Obviously the bulk water in the central parts of the cavities as the major source of signal surpasses the relaxation effect which could be present in true microporous structures. Another error source is the relatively large 2-D voxel volume ($78*78*200\,\mu m^3$) which may contain several separate solid structures and lead to partial volume effects. Surface induced relaxation is noticed as in theory [16], the contours of short T_1 and T_2 relaxation time constants are limited to solid-liquid boundaries. In the case of T_1 relaxation the time constants at cancellous bone region vary from 1000 ms of cavity centers to 100 ms of solid surfaces. When the transverse T_2 relaxation is considered the corresponding values are 20 ms and 5 ms, respectively.

Relaxation constant mapping is important on the aspect of the quantification of NMR data. The measured T_2 relaxation constants suggest that reliable imaging of trabecular system demands an imaging sequence where the time-to-echo is as short as possible. In practice a spin-echo 3-D sequence with hard exciting and refocusing pulses is favored. If the sole trabecular structure is wanted to be visualized, the required recovery delay can be adjusted to fit the T_1 relaxation time constant of solid-

TABLE II Size distribution data for connectivity centers

	$C^A/\mu m^1$	$C^B/\mu m^1$	$\omega^A/\mu m^2$	$\omega^B/\mu m^2$	% of all centers *A*	% of all centers *B*
Sham	85	125	44	78	40.5	59.5
Ovx	90	146	47	84	45.7	54.3
C1	84	136	31	85	24.5	75.5

[1] $C^{A,B}$ mean size of connectivity centers in trabecular system *A*, *B*
[2] $\omega^{A,B}$ width of the gaussian distribution for centers in system *A*, *B*.

TABLE III Size distribution data for connecting throats

	$T^A/\mu m^3$	$T^B/\mu m^3$	$\omega^A/\mu m$	$\omega^B/\mu m$	% of all throats *A*	% of all throats *B*
Sham	39	75	19	71	27.6	72.4
Ovx	38	91	16.5	64	27.5	72.5
C1	39	96	17	54	29.5	70.5

[3] $T^{A,B}$ mean size of connecting throats in trabecular system A, B; $\omega^{A,B}$ width of the gaussian distribution for throats in system *A*, *B*.

liquid boundary. The recovery delay of 500 ms in this study exceeds the required value and the experimental time can be greatly reduced by using shorter recovery delays. Naturally this will lead to even stronger T_1 weighing in the image, but mainly in the regions of lesser interest.

4. Discussion

When the studied system contains an appropriate NMR active nucleus the major limitation of NMR microscopy in the structural research of porous media is the achievable image resolution. Generally, according to DeHoff *et al*. [18] the spacing between successive sections must be between a third and a tenth of the intercept length of the details of interest to determine topological properties as connectivity between objects. Some of the structural parameters to be defined, especially trabecular thickness and structural anisotropy are known to be strongly resolution dependent [15]. In a rat femur the trabecular thickness is in the range of 50–100 μm with trabecular separation of 180 μm or less [6, 8–10]. When we consider these values with the typical 3-D voxel size of 20*20*35 μm of this study, the clustering process of surface representation is expected to produce reliable results in the estimation of cancellous bone volume. If the details of structures are in the range of image resolution, the surface rendering process is expected to misinterpret the cancellous bone volume based on partial volume effects. Therefore some knowledge of structural characteristics of the sample are needed before imaging experiments.

Slice images of 3-D data set (Fig. 1(a)–(d)) with the current resolution are of relatively good quality and give a distinct view on the state of cancellous and cortical bone. The preservative effect of clodronate treatment on osteopenic bone is also observed. A major problem with the current 3-D setup is the required long experimental time. Despite this, 3-D spin-echo sequence was chosen as the standard imaging tool. More appropriate, faster experiments are needed for clinical studies, from the point of view of the 3-D connectivity analysis the experimental method is not essential.

The surface representation gives an estimate of cancellous bone volume with reasonable results of the relative loss of bone mass during osteopenia. When the 3-D NMR imaging results of this study are compared with previous results of similar systems from 2-D histomorphometry as a standard method [6, 8, 9, 11] and from 3-D X-ray microscopy [7], the cancellous bone volume is observed to be on the same level.

Connectivity analysis divides the trabecular network into connectivity centers and connecting throats. In standard histomorphometric analysis the quantity describing the fragment size of trabecular system is trabecular thickness. ConAn carries more information and this paper demonstrates the ability to express the trabecular system by size distributions of structural components. The analysis also proposed that the studied volumes contained two different trabecular systems, *A* and *B*, differing in the size of structural details. The response of systems to osteopenic degradation is also slightly different. The interconnectivity of the trabecular network is seen to decrease due to osteopenia. This analysis method offers an alternative way to study the structure of bone, in fact any porous media at a level of the resolution of imaging. Due to the demonstrative nature of this study no mechanical or histomorphometric studies are included.

Compared to bulk water the heterogeneous media induces fast relaxation. The relaxation effect arises from two origins. Firstly, water can be physically adsorbed on solid surface, remaining collagens or in micropores. In this case the expected relaxation rate should be fast on the terms of molecular mobility [17]. Secondly, the susceptibility contrast on solid-liquid boundary leads to local field inhomogeneities and fast transversal relaxation of the fluid [19], which is likely to be the dominating effect. When the time-to-echo in our 3-D imaging experiments was 4.37 ms, it is quite easy to imagine that strong surface relaxation effects produce a dramatic loss in the echo signal intensity. In practice, reliable imaging and connectivity analysis need as short time-to-echo as possible. On the other hand, the fast longitudinal relaxation in trabecular matrix gives a possibility to perform relatively fast imaging.

5. Conclusions

In summary, MR imaging can produce three-dimensional, microscopy range images on the cancellous bone structures. Structural properties of healthy, osteopenic and clodronate treated samples are clearly visible in slice images. Some topological trends of the architecture of bone can be seen and MR microimaging is expected to further highlight the solid structure in cases where the detail size to image resolution ratio is small enough. One of the problems with high-resolution MR imaging is the long experimental time and *in vivo* applications will most probably be limited to typically used single slice MR images. The evident benefit of MR microscopy compared to histomorphometry is that after the bone sample has been dissected and cut to fit the sample tube, no further slicing, meaning no mechanical stress, to sample is produced.

References

1. B. L. RIGGS and L. J. MELTON, III, *N. Engl. J. Med.* **314** (1986) 167.
2. S. PHILLIPS, N. FOX, F. J. JACOBS and W. E. WRIGHT, *Bone* **9** (1986) 27.
3. T. J. BECK, C. B. RUFF, W. W. SCOTT JR, C. C. PLATO, J. D. TOBIN and C. A. QUAN, *Calcif. Tissue Int.* **50** (1992) 24.
4. C. M. BAGI, D. WILKIE, K. GEORGELOS, D. WILLIAMS and D. BERTOLINI, *Bone* **21** (1997) 261.
5. T. J. WRONSKI and C. F. YEN, *Cells Mater*. Supp. 1 (1991) 69.
6. A. M. PARFITT, in ''Bone Histomorphometry: Techniques and Interpretation'' edited by R. R. Recker, (CRC Press Inc., Boca Raton, FL, 1983) pp. 143–223.
7. J. H. KINNEY, N. E. LANE and D. L. HAUPT, *J. Bone Minen. Res.* **10** (1995) 264.
8. K. KIPPO, R. HANNUNIEMI, L. LAURÉN, Z. PENG, P. KUURTAMO, T. VIRTAMO, P. ISAKSSON, T. OSTERMAN, H. K. VANNANEN, R. SELLMAN. *Bone* **23** (1998) 333.
9. H. B. WAYNFORTH, ''Experimental and surgical technique in the rat'', (San Diego, Academic Press, 1980).
10. C. M. BAGI, E. DELEON, R. BROMMAGE, D. ROSEN and A. SOMMER, *Calcif. Tissue Int.* **57** (1995) 40.

11. K. KIPPO, R. HANNUNIEMI, P. ISAKSSON, L. LAUREN, T. OSTERMAN, Z. PENG, J. TUUKKANEN, P. KUURTAMO, H. K. VAANANEN and R. SELLMAN, *J. Bone Miner. Res.* **13** (1998) 287.
12. J. L. ACKERMAN and L. GARRIDO, in the Seventh Annual Meeting, Society of Magnetic Resonance in Medicine, San Francisco, CA, USA, August 22–26, 1988, Abstracts, 195.
13. R. GLANTZ, PhD Thesis, Univ. Karlsruhe, 1997.
14. R. GLANTZ, *Bruker Report* **146** (1998) 26.
15. M. KOTHARI, T. M. KEAVENY, J. C. LIN, D. C. NEWITT, H. K. GENANT and S. MAJUMDAR, *Bone* **22** (1998) 437.
16. P. T. CALLAGHAN, ''Principles of nuclear magnetic resonance microscopy'' (Clarendon Press, Oxford, 1991).
17. B. P. HILLS, K. M. WRIGHT and J. E. M. SNAAR, *Magn. Reson. Imaging* **14** (1996) 715.
18. R. T. DEHOFF, E. H. AIGELTINGER and K. R. CRAIG, *J. Microsc.* **95** (1972) 69.
19. S. BOBROFF and G. GUILLOT, *Magn. Reson. Imaging* **14** (1996) 819.

Received 30 December 1999
and accepted 2 March 2000